Acta Crystallographica Section D
Biological Crystallography
ISSN 0907-4449

Structure of the aspartic protease plasmepsin 4 from the malarial parasite *Plasmodium malariae* bound to an allophenylnorstatine-based inhibitor

José C. Clemente,[a]‡ Lakshmanan Govindasamy,[a]‡ Amrita Madabushi,[a] S. Zoë Fisher,[a] Rebecca E. Moose,[a] Charles A. Yowell,[b] Koushi Hidaka,[c] Tooru Kimura,[c] Yoshio Hayashi,[c] Yoshiaki Kiso,[c] Mavis Agbandje-McKenna,[a] John B. Dame,[b] Ben M. Dunn[a] and Robert McKenna[a]*

[a]Department of Biochemistry and Molecular Biology, College of Medicine, University of Florida, USA, [b]Department of Pathobiology, College of Veterinary Medicine, University of Florida, USA, and [c]Department of Medicinal Chemistry, Center for Frontier Research in Medicinal Science, Kyoto Pharmaceutical University, Yamashina-ku, Kyoto 607-8412, Japan

‡ These authors contributed equally to this work.

Correspondence e-mail: rmckenna@ufl.edu

Received 30 September 2005
Accepted 8 December 2005

PDB Reference: *P. malariae* plasmepsin 4, 2anl, r2anlsf.

The malarial parasite continues to be one of the leading causes of death in many developing countries. With the development of resistance to the currently available treatments, the discovery of new therapeutics is imperative. Currently, the plasmepsin enzymes found in the food vacuole of the parasite are a chief target for drug development. Allophenylnorstatine-based compounds originally designed to inhibit HIV-1 protease have shown efficacy against all four plasmepsin enzymes found in the food vacuole of *Plasmodium falciparum*. In this study, the first crystal structure of *P. malariae* plasmepsin 4 (PmPM4) bound to the allophenylnorstatine-based compound KNI-764 is described at 3.3 Å resolution. The PmPM4–inhibitor complex crystallized in the orthorhombic space group $P2_12_12$, with unit-cell parameters $a = 95.9$, $b = 112.6$, $c = 90.4$ Å, with two molecules in the asymmetric unit related by a non-crystallographic symmetry operator. The structure was refined to a final R factor of 24.7%. The complex showed the inhibitor in an unexpected binding orientation with allophenylnorstatine occupying the S1′ pocket. The P2 group was found outside the S2 pocket, wedged between the flap and a juxtaposed loop. Inhibition analysis of PmPM4 also suggests the potential for allophenylnorstatine-based compounds to be effective against all species of malaria infecting humans and for the future development of a broad-based inhibitor.

1. Introduction

It is estimated that at any one time there are about 300 million people infected with malaria worldwide. There are four species of malaria that infect humans: *Plasmodium falciparum* (Pf), *P. malariae* (Pm), *P. ovale* (Po) and *P. vivax* (Pv). Pf is responsible for the majority of deaths associated with malarial infections, while Pm, Po and Pv are associated with causing a chronic infection, in some cases for an individual's entire life. These chronic diseases are quite debilitating and are a major drain on the resources and manpower of developing countries (World Health Organization; http://www.who.int/en/). The current spread of malarial strains resistant to existing therapeutics emphasizes the need to develop new treatment options.

During the asexual stage of the parasite life cycle, it invades red blood cells and degrades hemoglobin. This is performed in a specialized compartment called the food vacuole (Francis *et al.*, 1997). The plasmepsin (PM) enzymes are key in the degradation of hemoglobin (Banerjee *et al.*, 2002). It has long been known that treating parasites in culture with aspartic protease inhibitors kills the parasite (Francis *et al.*, 1994; Haque *et al.*, 1999; Nezami & Freire, 2002; Rosenthal, 1995).

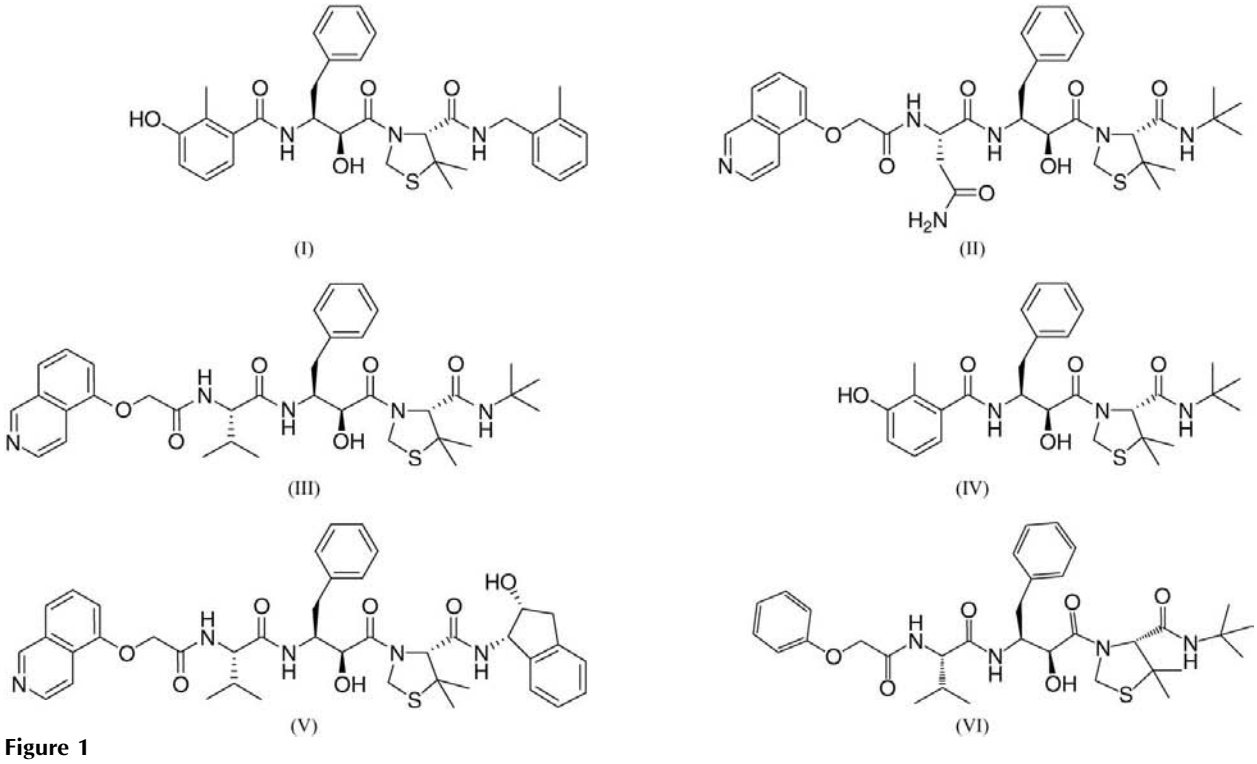

Figure 1
Structures of inhibitors listed in Table 1.

This fact, along with their key function in hemoglobin degradation, makes the plasmepsin enzymes viable drug targets (Coombs *et al.*, 2001). Pf contains four plasmepsin enzymes in the food vacuole: PfPM1, PfPM2, histoaspartic protease (HAP) and PfPM4 (Banerjee *et al.*, 2002). The PfPM1 and PfPM2 enzymes have 73% sequence identity and have approximately 64% identity with PfPM4 and 60% identity with HAP, but have only about 35% identity with the human aspartic protease cathepsin D (Francis *et al.*, 1994). The food vacuole of other malarial species contain only one aspartic protease, an ortholog of PfPM4 (PvPM4, PmPM4 and PoPM4 in Pv, Pm and Po, respectively; Dame *et al.*, 2003). PmPM4 shows 75% identity to PfPM4 (Bernstein *et al.*, 2003). This suggests that PM4 is a critical enzyme and targeting this enzyme may inhibit all or three of the four species, since there is evidence for redundancy in Pf. There is a concern that with Pf all four plasmepsin enzymes might have to be targeted to effectively inhibit the parasite (Omara-Opyene *et al.*, 2004). Since Pv, Pm and Po only contain one plasmepsin enzyme in their food vacuole, this concern is lessened.

There are currently available in the Protein Data Bank nine PfPM2, one PfPM4 and two PvPM4 structures (Asojo *et al.*, 2002, 2003; Bernstein *et al.*, 1999, 2003; Prade *et al.*, 2005; Silva *et al.*, 1996). In this study, we report the first crystal structure of PmPM4 and the first structure of a plasmepsin enzyme bound to an allophenylnorstatine-based inhibitor, KNI-764, also known as AG1776 and JE-2147. This class of inhibitor has been shown to be effective against the Pf food-vacuole enzymes (Nezami *et al.*, 2002, 2003). KNI-764 binds PmPM4 in an unexpected orientation compared with that previously modeled (Abdel-Rahman *et al.*, 2004). Inhibition analysis of

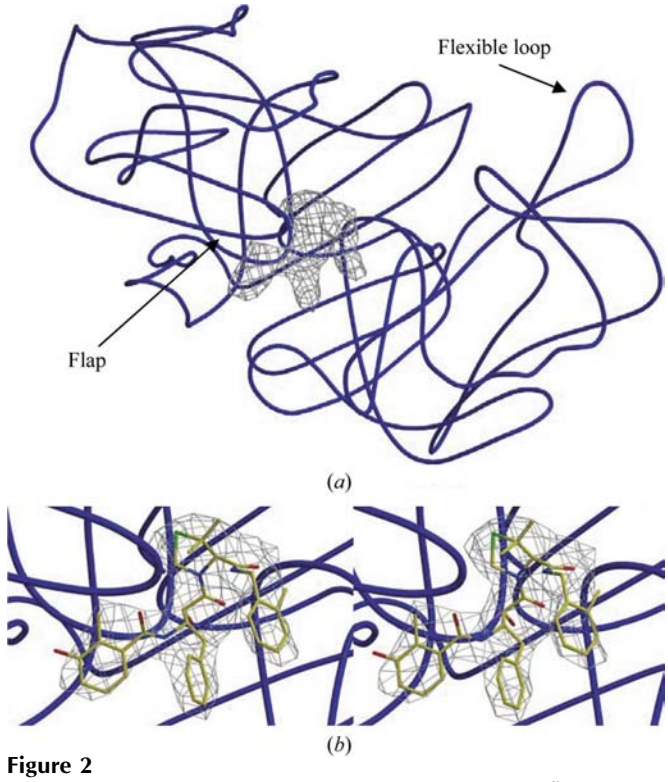

Figure 2
(*a*) Ribbon diagram of the PmPM4 homology model C^{α} coordinates (blue) used for molecular replacement, generated using the PfPM4–pepstatin A complex structure (Asojo *et al.*, 2003), with the pepstatin A and solvent molecules removed to prevent model bias. (*b*) Close-up stereoview of the initial $|F_o| - |F_c|$ electron-density omit map (grey), contoured at 2.5σ, and the fit of the inhibitor KNI-764 (in ball-and-stick representation with C, N, O and S atoms in yellow, blue, red and green colours, respectively) coordinates. This figure was generated with *BobScript* (Esnouf, 1999) and *RASTER3D* (Merritt & Bacon, 1997).

Table 1
Inhibition analysis.

Inhibitor (see Fig. 1)	KNI	K_i (n*M*)
I	764†	110 ± 10
II	223	7100 ± 900
III	492	3000 ± 500
IV	577	3000 ± 250
V	1622	25 ± 3
VI	10056	160 ± 30

† Inhibitor crystallized in this study.

PmPM4 with additional allophenylnorstatine-based inhibitors along with structural information provides insight for future drug design.

2. Materials and methods

2.1. Protein expression and purification

The proenzyme form of PmPM4 was overexpressed using the pET3a vector (Novagen) in *Escherichia coli* BL21(DE3) pLysS cells. Protein purification, isolation of inclusion bodies, refolding and purification were performed as described for PfPM2 (Westling *et al.*, 1997, 1999). The purified proenzyme was incubated with 20 m*M* sodium formate pH 4.4 for 5 min at 310 K. The enzyme solution was then returned to pH 8.0 with the addition of 20 m*M* Tris. Activated PmPM4 was first purified by ion exchange using a Hi-Trap HP column (Amersham). The protease was eluted off the column with buffer containing 20 m*M* Tris pH 8 and 1 *M* NaCl. The activated protease was further purified by size-exclusion chromatography using a Superdex 75 16/60 column (Amersham) using 20 m*M* Tris pH 8.0.

2.2. Inhibition analysis

Kinetic analysis was performed using a Cary 50 BIO UV–visible spectrophotometer with an 18-cell transporter at 310 K. Proenzyme was activated by incubation for 5 min in 0.1 *M* sodium formate pH 4.4 at 310 K prior to mixing with the chromogenic substrate KPIEF*NphRL. To determine K_i values, at least six different substrate concentrations were used and cleavage rates were measured with a minimum of two concentrations of inhibitor. Analysis was performed with the *Enzyme Kinetics Module* v.1.0 for *Sigma Plot* 2000. K_i values were determined for each inhibitor from a global fit of the curves with and without inhibitor using the equation $v = V_{max}/[1 + (K_m/S)(1 + I/K_i)]$.

2.3. Crystallization and structure determination

PmPM4 was crystallized as described previously in Madabushi *et al.* (2005). Briefly, crystals of PmPM4 complexed with the allophenylnorstatine-based compound KNI-764 were obtained at room temperature using the hanging-drop vapor-diffusion method. The inhibitor was dissolved in 100% DMSO at a concentration of 20 m*M* and preincubated with enzyme in a 20:1 ratio prior to crystallization. The reservoir solution contained 0.2 *M* ammonium sulfate and 15% PEG 4000 as precipitant. Crystals were grown by mixing 10 µl protein–inhibitor complex and 4 µl reservoir solution and suspending the drop over 1000 µl reservoir solution. Although crystallization of PmPM4 preincubated with all the allophenylnorstatine-based compounds given in Table 1 and shown in Fig. 1 were attempted, useful crystals were only obtained with KNI-764 complexed.

Crystals were flash-frozen at 100 K using 30% glycerol as a cryoprotectant prior to data collection. The intensity data were collected using an in-house Rigaku HU-H3R Cu rotating-anode generator and R-AXIS IV^{++} image-plate system and were integrated and scaled using the programs *DENZO* and *SCALEPACK* from the *HKL* suite (Otwinowski & Minor, 1997). The crystals belong to the orthorhombic space group $P2_12_12$, with unit-cell parameters a = 95.9, b = 112.6, c = 90.4 Å, with two molecules in the crystallographic asymmetric unit related by a non-crystallographic symmetry (NCS) operator. Initial phases were calculated by the molecular-replacement method using the program *MOLREP* (Vagin & Teplyakov, 1997). The PmPM4 homology model coordinates were generated using a PfPM4–pepstatin A complex structure (Asojo *et al.*, 2003), with the pepstatin A and solvent molecules removed to prevent model bias (Fig. 2*a*). The molecular-replacement solutions of the two molecules (*A* and *B*) in the crystallographic asymmetric unit were subjected to rigid-body refinement to optimize both orientation and position. The NCS operator was then defined and molecule *A* was used in all further refinement protocols using the *CNS* and *REFMAC* refinement packages (Brünger *et al.*, 1998; Murshudov *et al.*, 1997). After one cycle of rigid-body refinement, annealing by heating to 3000 K with gradual cooling, geometry-restrained position refinement and temperature-factor refinement, the generated $F_o - F_c$ Fourier omit map clearly and unambiguously showed, given the strong electron density indicating the location of the S atom, the position and orientation of the KNI-764 inhibitor (Fig. 2*b*). Interactive model building was performed using the graphics program *Coot* (Emsley & Cowtan, 2004).

3. Results and discussion

3.1. Structural analysis

The crystal structure of PmPM4 in complex with an allophenylnorstatine-based inhibitor was solved by the molecular-replacement method and refined to a resolution of 3.3 Å. The plasmepsin was crystallized in space group $P2_12_12$, with two molecules in the crystallographic asymmetric unit. The structure was refined to a final R factor of 24.7%. The bond geometries and φ/ψ values were shown to conform to standard values (Table 2).

The PmPM4 enzyme contains 326 residues and is folded into two almost equal size N- and C-terminal domains (Fig. 3*a*). The juncture of these two domains forms the floor of the active site containing the catalytic residues Asp34 and Asp214. The N-terminal domain contains a β-hairpin structural motif,

Table 2
X-ray data-collection and refinement statistics.

Values in parentheses are for the highest resolution shell.

Space group	$P2_12_12$
Unit-cell parameters (Å)	a = 95.9, b = 112.6, c = 90.4
Resolution (Å)	25.0–3.30 (3.38–3.30)
No. of unique reflections	14334
Completeness (%)	94.0 (82.2)
R_{sym}† (%)	10.4 (25.9)
$\langle I/\sigma(I)\rangle$	14.4 (3.8)
Phasing	*MOLREP*
Refinement	*CNS*/*REFMAC*5
R factor‡ (%)	24.7 (30.8)
R_{free}§ (%)	29.8 (38.6)
No. of protein atoms	2616
No. of water molecules	7
R.m.s.d. bond length (Å)	0.025
R.m.s.d. bond angle (°)	2.11
Average B factors (Å^2)	
Protein	55.4
KNI-764	52.7
Solvent	53.5
Ramachandran plot (%)	
Most favored regions	71.4
Additional allowed regions	25.9
Generously allowed regions	2.4
Disallowed regions	0.3

† $R_{sym} = \sum|I - \langle I\rangle|/\sum I \times 100$, where I is the intensity of a reflection and $\langle I\rangle$ is the average intensity. ‡ R factor $= \sum||F_o| - k|F_c||/\sum|F_o| \times 100$. § R_{free} is calculated from 5% randomly selected data for cross-validation.

which is called the 'flap' and caps the substrate-binding pocket.

The overall structural arrangement of the enzyme compares well with other reported inhibited plasmepsin structures (Fig. 3*b*). The crystal structures of known plasmepsin complexes were superimposed with the PmPM4 complex structure and resulted in r.m.s. deviations of 0.98 Å for 326 C$^\alpha$ atoms (PDB code 1qs8; PvPM4–pepstatin A), 0.96 Å for 320 C$^\alpha$ atoms (PDB code 1ls5; PfPM4–pepstatin A) and 1.26 Å for 320 C$^\alpha$ atoms (PDB code 1lf3; PfPM2–Eh58).

The residues from Val236 to Tyr245, known as the 'flexible loop', are ordered but exhibit different conformations in the plasmepsin structures (Fig. 3*a*). In addition to this large loop variation, two other flexible loop regions, residues 277–282 and 292–299, displayed conformational differences (∼1.5–3.0 Å) when compared between the plasmepsin enzymes.

The KNI inhibitor series is based on the allophenylnorstatine core. These inhibitors were originally designed to inhibit HIV-1 protease (Kiriyama *et al.*, 1993; Kiso, 1993; Kiso *et al.*, 1999; Mimoto *et al.*, 1991, 1992). The allophenylnorstatine core is meant to mimic the unique Phe-Pro cleavage sites found in the GagPol polyprotein. Utilizing this unique cleavage-site sequence provides specificity against the HIV protease over the human aspartic proteases. These inhibitors have also been shown to have good bioavailability and low toxicity (Kiriyama *et al.*, 1996). Nezami and coworkers later showed that the similarity to the cleavage site in hemoglobin (Phe-Leu) cleaved by the plasmepsin enzymes would also make the KNI series of inhibitors effective against the malarial parasite (Nezami *et al.*, 2002).

In this study, we crystallized the inhibitor KNI-764 with PmPM4 and analyzed the binding of five additional related inhibitors. KNI-764 contains the allophenylnorstatine-thioproline core spanning the S1–S1′ pockets. In the structure of this inhibitor bound to the HIV-1 protease the (*R*)-5,5-dimethyl-1,3-thiazolidine-4-carboxylic acid (Dmt) occupies the S1′ pocket and the allophenylnorstatine group occupies the S1 pocket (Reiling *et al.*, 2002). The S2 pocket is occupied by the 3-hydroxy-2-methylbenzoyl group and the S2′ pocket is occupied by the 2-methylbenzylamine group. Structural alignment of the PmPM4 and HIV-1 complexes with KNI-764, based on the position of the inhibitors and the catalytic aspartic acids, shows similar positioning of the inhibitors. The only significant difference between the two complexes was the 2-methylbenzylamine group conformation, even though the proteases show little sequence similarity.

Based on the structural alignments of the C$^\alpha$ coordinates of PmPM4–KNI-764 with those of the PvPM4–pepstatin and PfPM4–pepstatin complexes, which gave r.m.s. deviations of 0.83 and 0.98 Å, respectively (Asojo *et al.*, 2003; Bernstein *et al.*, 2003; Fig. 3*b*), the KNI-764 inhibitor occupies the active site of the PmPM4 protease in an unexpected conformation. Unlike in the HIV-1 protease, the Dmt group occupies the S1 pocket and the allophenylnorstatine group occupies the S1′ pocket, as shown by the alignment with pepstatin (Fig. 4). The 5,5-dimethyl substitution on the Dmt group makes close interactions with the flap (Fig. 5*a*). Although the Dmt group does fit well into the S1 pocket, it does not occupy the S1 pocket fully. Using a combinatorial substrate approach, Beyer and coworkers showed that the preferred residue in the S1 pocket is Phe (Beyer *et al.*, 2005). This pocket shows strong specificity for Phe and Leu over all other residues. These two residues would be able to extend and fill the S1 pocket and correlate well with the deep hydrophobic pocket seen in the PmPM4 protease. The allophenylnorstatine occupying the S1′ pocket makes hydrophobic interactions with residues Phe192, Leu294 and Leu300 (Fig. 5*b*). The study by Beyer and coworkers also showed that the preferred residue in the S1′ pocket is Phe. This suggests that the binding orientation of the inhibitor is being determined by the allophenylnorstatine group and the preferences of the S1′ pocket.

The 2-methylbenzylamine is designated as the P2 group based on the position of the Dmt group, but it does not occupy the S2 pocket (Fig. 5*a*). The 2-methylbenzylamine is wedged between the flap (residues Val73–Arg83) and a juxtaposed loop (residues Met286–Asp295), making hydrophobic contact with residues Val292, Ile300, Gly78 and Ser79. Substrate analysis showed that the S2 pocket has a preference for Glu, suggesting a preference for charged groups. The S2 pocket is lined by Thr219, Thr217 and Thr221, three potential hydrogen-bond donors and acceptors. A hydrogen bond is formed between the backbone O23 of KNI-764 and Thr217 (Fig. 5*c*). The preferences for this pocket are discussed further below.

The S2′ pocket is occupied by the 3-hydroxy-2-methylbenzoyl group. The S2′ pocket is highly hydrophobic and has shown a preference for large hydrophobic residues (Beyer *et*

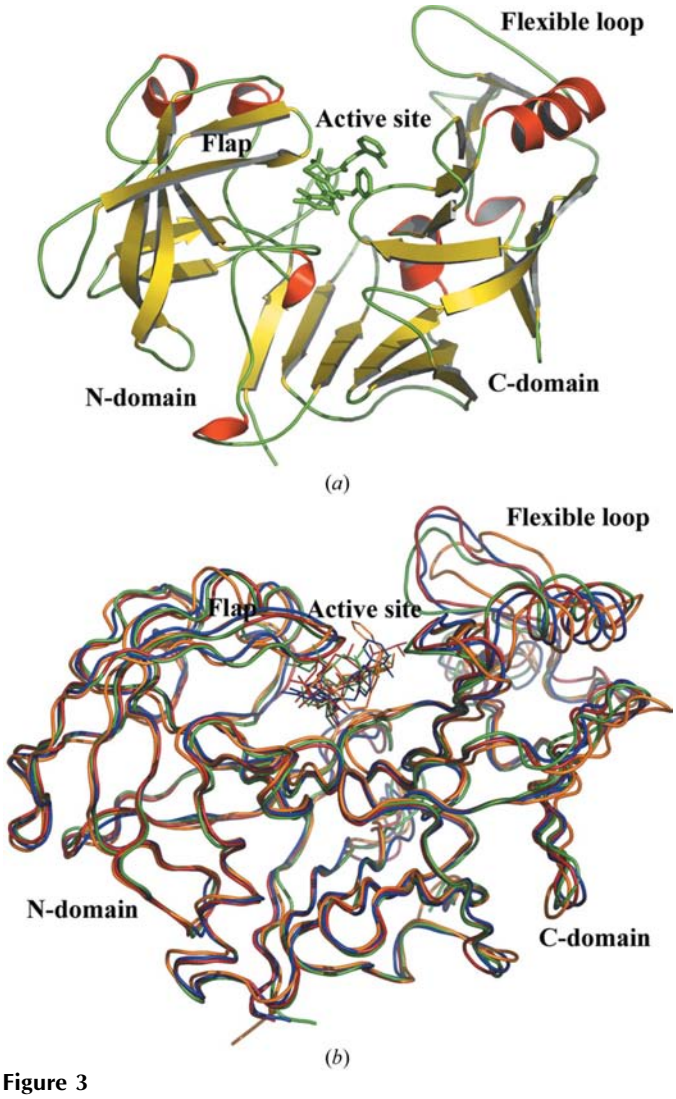

Figure 3
(*a*) Ribbon diagram of the PmPM4–KNI-764 complex. The PmPM4 β-strands, coil and helices are colored yellow, green and red, respectively. KNI-764 is depicted in green sticks. (*b*) Structural superposition of the C^{α} trace of PmPM4–KNI-764 (blue), PvPM4–pepstatin A (red; Bernstein *et al.*, 2003), PfPM4–pepstatin A (green; Asojo *et al.*, 2003) and PfPM2–Eh58 (orange; Asojo *et al.*, 2003). This figure was generated using *PyMOL* (DeLano, 2002).

al., 2005). The 3-hydroxy-2-methylbenzoyl occupies the S2′ pocket, making hydrophobic contacts with residues Leu131 and Tyr192. A water-mediated hydrogen bond is also found between O2 of the P2 group and the Thr76 carbonyl (Fig. 5*c*). The S2′ pocket is left mainly unoccupied and can potentially accommodate larger side chains. The S2′ pocket is also lined by potential hydrogen-bond donors and acceptors, Asn39 and Ser37.

A total of five potential hydrogen-bond interactions are observed between KNI-764 and PmPM4. Two are between the catalytic residues Asp34 and Asp214 and the KNI-764 O21 atom (Fig. 5*c*); these exhibit similar distances to those observed in other known plasmepsin–inhibitor complex structures. A third is between the KNI-764 O10 atom and Gly78 in the flap; the fourth and fifth have been discussed above.

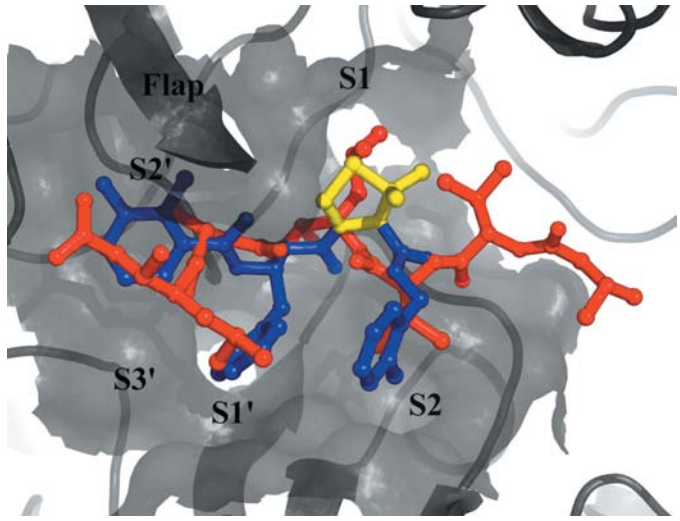

Figure 4
C^{α} overlap of PmPM4–KNI-764 (KNI-764 in blue with the Dmt group in the S1 pocket in yellow) and PfPM4–pepstatin (red). The ribbon and Connolly surface of PmPM4 is drawn in gray.

3.2. Inhibition analysis

KNI-764 showed a dissociation constant (K_i) for inhibition of 110 $\pm$ 10 n*M* (Table 1). Based on the structural data, we further analyzed the inhibition preferences of PmPM4, specifically focusing on the S2 and S2′–S3′ pockets. Replacing the 2-methylbenzylamine at P2 by the *t*-butyl group (KNI-577) decreased the binding affinity by >25-fold. This correlates well with the previous work performed with PfPM2 (Nezami *et al.*, 2002). This suggests that the binding mechanism for PfPM2 is similar to that for PmPM4. Extending the inhibitor by placing Val at P2′ and an isoquinolinyloxyacetyl group at P3′ did not improve inhibition (KNI-492). Analysis of the structure suggested that the S2′ pocket would be accommodating to hydrogen-bond donors and acceptors. Replacing Val with Asn at P2′ further decreased the binding affinity by twofold. This suggests that Asn is unable to reach into the S2′ pocket and create charged interactions with Asn39 and Ser37 and is also unable to make hydrophobic interactions with Leu131 and Phe192, potentially creating a charge–hydrophobic clash. Replacement of isoquinolinyloxyacetyl (KNI-492) by phenoxyacetyl (KNI-10056) increased the binding affinity by ~20-fold. The smaller phenyl group may allow greater access to the backbone O atoms of the phenoxyacetyl in KNI-10056 for hydrogen bonding. This correlates well with the studies on PfPM2, which has a preference for small hydrophobic groups in this region, and the combinatorial substrate library results, which showed Ile as the best residue for P3′ (Beyer *et al.*, 2005; Nezami *et al.*, 2002). When the *t*-butyl group (KNI-492) in P2 is replaced by (1*S*,2*R*)-1-amino-2-indanol (KNI-1622), the binding affinity is improved by >115-fold. KNI-1622 showed the best inhibition of PmPM4, with a K_i of 25 $\pm$ 3 n*M*. This is an improvement in binding affinity of fourfold compared with KNI-764. These results are also in agreement with the study by Nezami and coworkers with PfPM4 and again suggest that the binding orientation of the allophenylnorstatine-based

inhibitors is similar for all plasmepsins (Nezami *et al.*, 2003).

4. Conclusions

The current study shows the first reported structure of PmPM4 and of an allophenylnorstatine-based inhibitor bound to a plasmepsin enzyme. This demonstrates that the inhibitor binds in an unexpected orientation with the allophenylnorstatine group in the S1′ pocket. Given the sequence and structural similarity between the plasmepsin enzymes, it would be expected that the other plasmepsins would also bind in the same orientation. This information sheds new light on the binding of allophenylnorstatine-based compounds and will aid in the design and modeling of future inhibitors. The current study also supports the ability of allophenylnorstatine-based inhibitors to adapt and inhibit not only the four enzymes found in the food vacuole of *P. falciparum*, but also to potentially inhibit the PfPM4 orthologs found in the other malarial species. Since the majority of the malaria-infected population lives in underdeveloped countries, the development of a broad-based inhibitor is essential to create an affordable drug.

The authors thank Dr Sibani Chakraborty for useful discussions. This work was supported by NIH grants AI39211 (JBD and BMD) and DK18865 (BMD), University of Florida College of Medicine start-up funds (RM) and a University of Florida opportunity fund (JBD, BMD and RM).

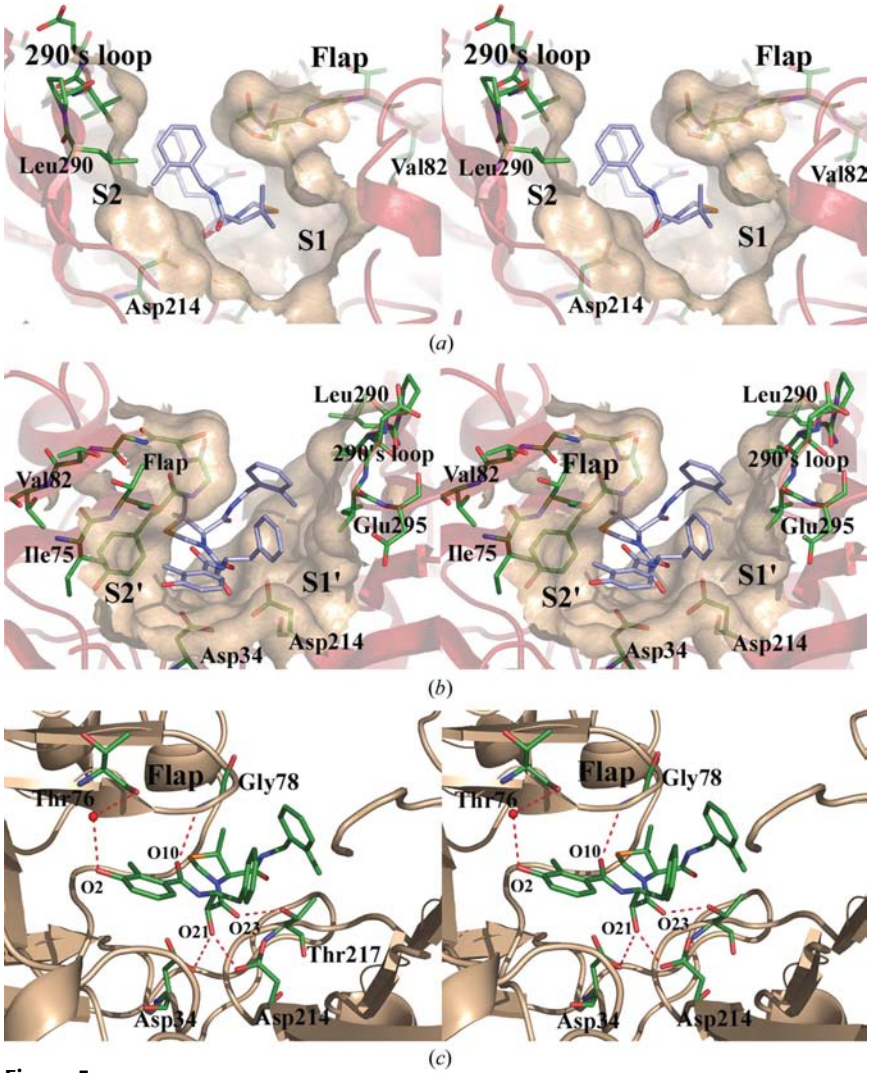

Figure 5
Stereoviews of KNI-764 in the active site of PmPM4. (*a*) View of P1 and P2 of KNI-764. (*b*) View of P1′ and P2′ of KNI-764. The surface of the active site is shown as a beige Connolly surface. PmPm4 is shown as a red ribbon. KNI-764 is modeled as blue sticks. The residues of the flaps (Ile75–Val82) and the 290s loop (Leu290–Glu295) are depicted as green sticks. (*c*) Plausible hydrogen-bonding interactions (red broken lines) between PmPM4 and KNI-764.

References

Abdel-Rahman, H. M., Kimura, T., Hidaka, K., Kiso, A., Nezami, A., Freire, E., Hayashi, Y. & Kiso, Y. (2004). *Biol. Chem.* **385**, 1035–1039.
Asojo, O. A., Afonina, E., Gulnik, S. V., Yu, B., Erickson, J. W., Randad, R., Medjahed, D. & Silva, A. M. (2002). *Acta Cryst.* D**58**, 2001–2008.
Asojo, O. A., Gulnik, S. V., Afonina, E., Yu, B., Ellman, J. A., Haque, T. S. & Silva, A. M. (2003). *J. Mol. Biol.* **327**, 173–181.
Banerjee, R., Liu, J., Beatty, W., Pelosof, L., Klemba, M. & Goldberg, D. E. (2002). *Proc. Natl Acad. Sci. USA*, **99**, 990–995.
Bernstein, N. K., Cherney, M. M., Loetscher, H., Ridley, R. G. & James, M. N. (1999). *Nature Struct. Biol.* **6**, 32–37.
Bernstein, N. K., Cherney, M. M., Yowell, C. A., Dame, J. B. & James, M. N. (2003). *J. Mol. Biol.* **329**, 505–524.
Beyer, B. B., Johnson, J. V., Chung, A. Y., Li, T., Madabushi, A., Agbandje-McKenna, M., McKenna, R., Dame, J. B. & Dunn, B. M. (2005). *Biochemistry*, **44**, 1768–1779.
Brünger, A. T., Adams, P. D., Clore, G. M., DeLano, W. L., Gros, P., Grosse-Kunstleve, R. W., Jiang, J.-S., Kuszewski, J., Nilges, M., Pannu, N. S., Read, R. J., Rice, L. M., Simonson, T. & Warren, G. L. (1998). *Acta Cryst.* D**54**, 905–921.
Coombs, G. H., Goldberg, D. E., Klemba, M., Berry, C., Kay, J. & Mottram, J. C. (2001). *Trends Parasitol.* **17**, 532–537.
Dame, J. B., Yowell, C. A., Omara-Opyene, L., Carlton, J. M., Cooper, R. A. & Li, T. (2003). *Mol. Biochem. Parasitol.* **130**, 1–12.
DeLano, W. L. (2002). *The PyMOL Molecular Graphics System.* http://www.pymol.org.
Emsley, P. & Cowtan, K. (2004). *Acta Cryst.* D**60**, 2126–2132.
Esnouf, R. M. (1999). *Acta Cryst.* D**55**, 938–940.
Francis, S. E., Gluzman, I. Y., Oksman, A., Knickerbocker, A., Mueller, R., Bryant, M. L., Sherman, D. R., Russell, D. G. & Goldberg, D. E. (1994). *EMBO J.* **13**, 306–317.
Francis, S. E., Sullivan, D. J. Jr & Goldberg, D. E. (1997). *Annu. Rev. Microbiol.* **51**, 97–123.
Haque, T. S., Skillman, A. G., Lee, C. E., Habashita, H., Gluzman, I. Y., Ewing, T. J., Goldberg, D. E., Kuntz, I. D. & Ellman, J. A. (1999). *J. Med. Chem.* **42**, 1428–1440.

Kiriyama, A., Mimoto, T., Kiso, Y. & Takada, K. (1993). *Biopharm. Drug Dispos.* **14**, 199–207.
Kiriyama, A., Sugahara, M., Yoshikawa, Y., Kiso, Y. & Takada, K. (1996). *Biopharm. Drug Dispos.* **17**, 125–134.
Kiso, Y. (1993). *Nippon Rinsho*, **51**, *Suppl.*, 139–145.
Kiso, Y., Matsumoto, H., Mizumoto, S., Kimura, T., Fujiwara, Y. & Akaji, K. (1999). *Biopolymers*, **51**, 59–68.
Madabushi, A., Chakraborty, S., Fisher, S. Z., Clemente, J. C., Yowell, C., McKenna-Agbandje, M., Dame, J. B., Dunn, B. M. & McKenna, R. (2005). *Acta Cryst.* F**61**, 228–231.
Merritt, E. A. & Bacon, D. J. (1997). *Methods Enzymol.* **277**, 505–524.
Mimoto, T., Imai, J., Kisanuki, S., Enomoto, H., Hattori, N., Akaji, K. & Kiso, Y. (1992). *Chem. Pharm. Bull. (Tokyo)*, **40**, 2251–2253.
Mimoto, T., Imai, J., Tanaka, S., Hattori, N., Kisanuki, S., Akaji, K. & Kiso, Y. (1991). *Chem. Pharm. Bull. (Tokyo)*, **39**, 3088–3090.
Murshudov, G. N., Vagin, A. A. & Dodson, E. J. (1997). *Acta Cryst.* D**53**, 240–255.
Nezami, A. & Freire, E. (2002). *Int. J. Parasitol.* **32**, 1669–1676.
Nezami, A., Kimura, T., Hidaka, K., Kiso, A., Liu, J., Kiso, Y., Goldberg, D. E. & Freire, E. (2003). *Biochemistry*, **42**, 8459–8464.
Nezami, A., Luque, I., Kimura, T., Kiso, Y. & Freire, E. (2002). *Biochemistry*, **41**, 2273–2780.
Omara-Opyene, A. L., Moura, P. A., Sulsona, C. R., Bonilla, J. A., Yowell, C. A., Fujioka, H., Fidock, D. A. & Dame, J. B. (2004). *J. Biol. Chem.* **279**, 54088–54096.
Otwinowski, Z. & Minor, W. (1997). *Methods Enzymol.* **276**, 307–326.
Prade, L., Jones, A. F., Boss, C., Richard-Bildstein, S., Meyer, S., Binkert, C. & Bur, D. (2005). *J. Biol. Chem.* **280**, 23837–23843.
Reiling, K. K., Endres, N. F., Dauber, D. S., Craik, C. S. & Stroud, R. M. (2002). *Biochemistry*, **41**, 4582–4594.
Rosenthal, P. J. (1995). *Exp. Parasitol.* **80**, 272–281.
Silva, A. M., Lee, A. Y., Gulnik, S. V., Maier, P., Collins, J., Bhat, T. N., Collins, P. J., Cachau, R. E., Luker, K. E., Gluzman, I. Y., Francis, S. E., Oksman, A., Goldberg, D. E. & Erickson, J. W. (1996). *Proc. Natl Acad. Sci. USA*, **93**, 10034–10039.
Vagin, A. & Teplyakov, A. (1997). *J. Appl. Cryst.* **30**, 1022–1025.
Westling, J., Cipullo, P., Hung, S. H., Saft, H., Dame, J. B. & Dunn, B. M. (1999). *Protein Sci.* **8**, 2001–2009.
Westling, J., Yowell, C. A., Majer, P., Erickson, J. W., Dame, J. B. & Dunn, B. M. (1997). *Exp. Parasitol.* **87**, 185–193.